

Propagating waves in bounded elastic media: Transition from standing waves to anguilliform kinematics

SOPHIE RAMANANARIVO, RAMIRO GODOY-DIANA and BENJAMIN THIRIA

Physique et Mécanique des Milieux Hétérogènes (PMMH), CNRS UMR 7636; ESPCI ParisTech; UPMC (Paris 6); Univ. Paris Diderot (Paris 7) - 10 rue Vauquelin, 75231 Paris, Cedex 5, France

received 5 March 2014; accepted 6 March 2014
published online 14 March 2014

PACS 46.40.-f – Vibrations and mechanical waves
PACS 87.85.gj – Movement and locomotion
PACS 47.85.-g – Applied fluid mechanics

Abstract – Confined geometries usually involve reflected waves interacting together to form a spatially stationary pattern. A recent study on bio-locomotion, however, has reported that propagating wave kinematics can naturally emerge in a forced elastic rod, even with boundary conditions involving significant reflections. It has been shown that this particular behavior is observed only in the presence of strong damping. Based on those observations, this study aims at giving a quantitative description of the mechanism involved to prevent the build-up of standing waves and generate traveling solutions. The question is discussed here in the framework of handmade artificial swimmers as an example of practical application but we believe that its potential is beyond this scope.

 Copyright © EPLA, 2014

Due to the presence of boundary conditions, traveling waves propagating in bounded media evolve into standing-wave solutions. A canonical textbook example is the wave pattern on a string. More generally, for elastic, capillary, or gravity waves, when the typical size of the system is comparable to the wavelength, the obtained pattern is thus determined by the way the different reflected waves interact, which is set by the geometry.

A recent study on bio-locomotion [1], though, has shown that even systems whose dynamics is strongly dependent on geometry (a beam, or a plate, for instance) can exhibit very different behaviors. The experiment consisted in an elastic rod placed on a water surface and subjected to harmonic forcing at one of its ends. The authors showed that, depending on the conditions, the dynamical response passes from classic standing waves to traveling solutions (see fig. 1). In the particular case of bio-inspired artificial eel-like swimmers, this transition controls the ability of the elastic body to achieve an anguilliform kinematics, thus affecting the global swimming efficiency [2–4]. This was an important result for optimizing artificial realizations of autonomous swimming propellers.

Concerning the underlying mechanism inducing this transition, they showed that those particular dynamical responses were only made possible by the presence of a

strong dissipation rate [1]. This dissipation is due to kinetic energy being wasted to the fluid through transversal flow separation at each stroke cycle [1,5]. Without this term, only standing waves could be observed. However, the understanding of this transition is still an open question. To our knowledge, the issue of spontaneous establishment of a propagative dynamics in bounded media received limited attention in the literature. In most studies, the desired undulatory motion is imposed actively, either through a continuous mechanical actuation analog to muscles along a fish backbone (see, *e.g.*, the Tuna-form robot of [6]), or by controlling the vibratory response of the flexible structure through a spatial distribution of external forces (see, *e.g.*, [7]). The latter requires an active tuning of the excitation (that is commonly applied at the boundaries) until a pure traveling wave is formed. The authors, however, underlined the difficulty to obtain a robust system [8].

In this paper, we provide a description of the transition from a standing wave to a traveling wave using an analytical model and controlled experiments. The geometry studied is a classical plate under local harmonic forcing, that is chosen as a standard model of continuous dynamical system. We show here that the presence of a strong damping term induces a complex coupling of waves along

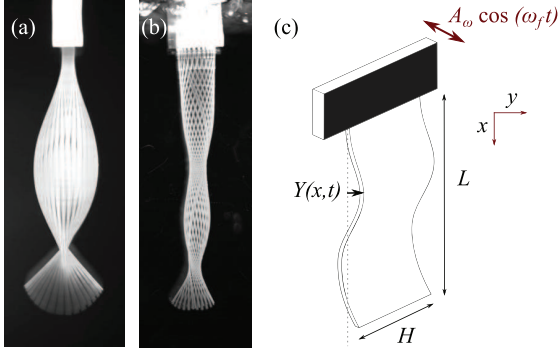


Fig. 1: (Colour on-line) Vibration experiments performed on a Mylar plate flapped with a shaker in air (a), and in water (b). In air, a standard standing-wave solution is observed, that is characteristic of systems influenced by the boundary conditions. In water, with a stronger damping, the plate now exhibits a traveling solution. (c) Model plate of finite length L , forced at its upper extremity.

the plate and generates a propagative kinematics. We confirm the importance of that transition for the optimization of artificial anguilliform swimmers.

Vibration experiments are performed using a rectangular Mylar plate (2×8 cm, thickness $150 \mu\text{m}$, $\mu = 4.1 \cdot 10^{-3} \text{ kg} \cdot \text{m}^{-1}$, and $B = 1.9 \cdot 10^{-5} \text{ N} \cdot \text{m}^2$), hanging vertically. The upper extremity of the elastic plate is clamped to a high-precision shaker whose frequency and amplitude are controlled. Under excitation, the system develops bending wave patterns that are visualized using a fast camera, and by illuminating the cross-section of the Mylar sheet with a laser. Recorded images are then post-treated with Matlab. The experiments are repeated in air and water, to cover different fluid dissipation rates. The recorded kinematics is observed to evolve from a standing wave in air, to a traveling solution in water (see fig. 1(a), (b)).

The plate is theoretically modeled as a linear Euler-Bernoulli beam [9] under harmonic forcing (see fig. 1(c)). In the absence of external flow, the action of the fluid has two main contributions, respectively through an added mass effect and a nonlinear dissipation due to cyclic flow separation [1,10,11]. The equation for the local transversal displacement $Y(x, t)$ writes

$$(\mu + M)\partial_t^2 Y + B\partial_x^4 Y + \alpha|\partial_t Y|\partial_t Y = 0, \quad (1)$$

where μ , M , B and α are, respectively, the mass per unit length of the plate, the added mass of fluid, the flexural bending rigidity of the plate and the damping coefficient. In addition, $Y(x, t)$ satisfies clamped-free boundary conditions: $Y(0, t) = A_\omega \cos(\omega_f t)$ and $\partial_x Y(0, t) = 0$ (where A_ω and ω_f are, respectively, the forcing amplitude and frequency), along with $\partial_x^2 Y(L, t) = \partial_x^3 Y(L, t) = 0$ (where L is the length of the plate). Using the typical length and time scales L and $L^2 \sqrt{(\mu + M)/B}$, eq. (1) yields in a dimensionless form

$$\partial_t^2 y + \partial_x^4 y + \tilde{\alpha}|\partial_t y|\partial_t y = 0, \quad (2)$$

with $\tilde{\alpha} = \alpha L/(\mu + M)$; the tilde denotes non-dimensionalized quantities. Equation (2) can be solved numerically, but in order to get a clearer view of the underlying physics, the nonlinear term on the left-hand side will be rewritten in a simplified linear form $\tilde{\alpha}|\partial_t y|\partial_t y \sim \tilde{\alpha}\tilde{A}_\omega\tilde{\omega}_f\partial_t y$ (with \tilde{A}_ω and $\tilde{\omega}_f$ the dimensionless forcing amplitude and frequency). By approximating the lateral speed by the maximal excitation value $\tilde{A}_\omega\tilde{\omega}_f$, the damping term will most probably be overestimated. However, this expression keeps the physical ingredients of a quadratic dissipation and allows to give a more straightforward description of our dynamical system. For the purpose of comparison, the analytical results will be plotted together with the nonlinear implementation of eq. (2) (*i.e.* including the exact expression of the damping term)¹. Therefore, the equation for the displacement y reads

$$\partial_t^2 y + \partial_x^4 y + \tilde{\alpha}\tilde{A}_\omega\tilde{\omega}_f\partial_t y = 0. \quad (3)$$

Assuming that the elastic response of the system is mainly described by $\tilde{\omega}_f$, we look for solutions $y(x, t) = \phi(x)e^{i\tilde{\omega}_f t}$; which gives

$$\partial_x^4 \phi - k^4 \phi = 0, \quad (4)$$

with the clamped-free boundary conditions $\phi(0) = \tilde{A}_\omega$, $\partial_x \phi(0) = \partial_x^2 \phi(1) = \partial_x^3 \phi(1) = 0$, and k that is determined by the complex dispersion relation

$$k^4 = \tilde{\omega}_f^2(1 - i\tilde{\alpha}\tilde{A}_\omega). \quad (5)$$

The solutions for ϕ are given by

$$\phi(x) = a_p^+ e^{-ikx} + a_p^- e^{ikx} + a_n^+ e^{-kx} + a_n^- e^{kx}, \quad (6)$$

where a_p^+ , a_p^- , a_n^+ and a_n^- are determined by the boundary conditions. Those constants are functions of \tilde{A}_ω and k (see footnote 2). Since k is a complex wave number, so are a_p^+ , a_p^- , a_n^+ and a_n^- . Thus, the function $\phi(x)$ describing the spatial variations of the lateral displacements $y(x, t)$ is now complex, which allows for a phase shift between the oscillating motion of each point along the plate. Writing $k = k_r + ik_i$ gives the following expression for $y(x, t)$:

$$y(x, t) = A_p^+(x)e^{i(\tilde{\omega}_f t - k_r x)} + A_p^-(x)e^{i(\tilde{\omega}_f t + k_r x)} + A_n^+(x)e^{i(\tilde{\omega}_f t - k_i x)} + A_n^-(x)e^{i(\tilde{\omega}_f t + k_i x)}, \quad (7)$$

¹Equation (2) is rewritten in a matrix form using finite differences and solved numerically in Matlab to obtain the complex amplitude $\phi(x)$, and subsequently the motion of the plate $y(x, t)$. The plate is discretized over 1000 points, which is sufficient to account for the spatial variations along its length. The actuation is imposed through the implementation of the boundary conditions.

²Exact expressions for the four constants a_p^+ , a_p^- , a_n^+ and a_n^- in eq. (6) are

$$\begin{aligned} a_p^+ &= \frac{\tilde{A}_\omega}{4} \left[\frac{1 + e^{ik}(\cosh k + i \sinh k)}{1 + \cos k \cosh k} \right], \\ a_p^- &= \frac{\tilde{A}_\omega}{4} \left[\frac{1 + e^{-ik}(\cosh k - i \sinh k)}{1 + \cos k \cosh k} \right], \\ a_n^+ &= \frac{1}{2} \left[\tilde{A}_\omega - (1 + i)a_p^+ - (1 - i)a_p^- \right], \\ a_n^- &= \frac{1}{2} \left[\tilde{A}_\omega - (1 - i)a_p^+ - (1 + i)a_p^- \right]. \end{aligned}$$

with the spatial envelopes

$$\begin{aligned} A_p^+(x) &= a_p^+ e^{k_i x}, & A_p^-(x) &= a_p^- e^{-k_i x}, \\ A_n^+(x) &= a_n^+ e^{-k_r x}, & A_n^-(x) &= a_n^- e^{k_r x}. \end{aligned} \quad (8)$$

As can be seen, the solution for the local displacement is expressed as the contribution of four waves. The first two terms in eq. (7) are propagative waves traveling forward and backward with a speed that depends explicitly on k_r . Their amplitudes as a function of x are given by the functions A_p^\pm (the sign refers to the direction of propagation). Those spatial envelopes vary over a characteristic lengthscale l_i (the inverse of k_i) associated to energy dissipation along the plate. l_i is here one order of magnitude larger than the spatial wavelength defined as $\lambda_r = 2\pi/k_r$. The last two terms of eq. (7) are near-field bending waves; these are evanescent waves that decay exponentially with the distance from the boundaries. As the spatial phase $k_i x$ is here varying slowly along the plate length ($k_i \ll k_r$), the contribution of these terms is essentially stationary and is not involved in the propagative mechanisms. This point is clearly evidenced observing fig. 2(f) (top and bottom) that details, respectively, the contribution of the first two terms of eq. (7) responsible for the traveling kinematics (top), and the stationary contribution of the last two terms (bottom).

Unlike the case with no friction ($k_i = 0$), there is now a possibility for a global propagation along the plate, which is conditioned by the balance between forward and backward contributions (*i.e.* the balance between the respective weights of the spatial functions A_p^+ and A_p^-). Figures 2(a)–(c) show the solution of eq. (7) for different friction rates $\tilde{\alpha}\tilde{A}_\omega$ (with the same non-dimensionalized forcing frequency, $\tilde{\omega}_f = 31$). The cases with no dissipation or intermediate dissipation are to be compared with experimental observations in air and water (the calculation of the experimental values of $\tilde{\alpha}\tilde{A}_\omega$ is described in footnote ³).

First, it is worth noting that for a value of $\tilde{\alpha}\tilde{A}_\omega = 0$ ($k_i = 0$), we retrieve the standard standing-wave solution of a conservative system with no friction (see fig. 2(a) and the supplementary [MovieS1.avi](#)). This case is compared to the vibration experiment performed in air for the same set of parameters. The observed kinematics (see fig. 2(d) and the supplementary [MovieS2.avi](#)) shows very good agreement with the theoretical one. Increasing $\tilde{\alpha}\tilde{A}_\omega$ (to 0.31) leads to the destabilization of the nodes and the emergence of a propagative component in the movement that is traveling forward (see fig. 2(b) and the supplementary [MovieS3.avi](#)). Again, this case shows strong similarities with the equivalent experimental measurements of a plate immersed in water (fig. 2(e) and supplementary

³Following [12], the added mass and the dissipation coefficient required to estimate the experimental value of $\tilde{\alpha} = \alpha L/(\mu + M)$ are taken to be $M = \rho\pi H^2/4$ and $\alpha = 1/2\rho C_d H$, with ρ the fluid density, H the height of the plate, and $C_d = 1.8$ the drag coefficient experimentally measured by [12]. The fluid dissipation rate associated to air and water are thus, respectively, $\tilde{\alpha}\tilde{A}_\omega = 2 \cdot 10^{-2}$ and $\tilde{\alpha}\tilde{A}_\omega = 0.31$.

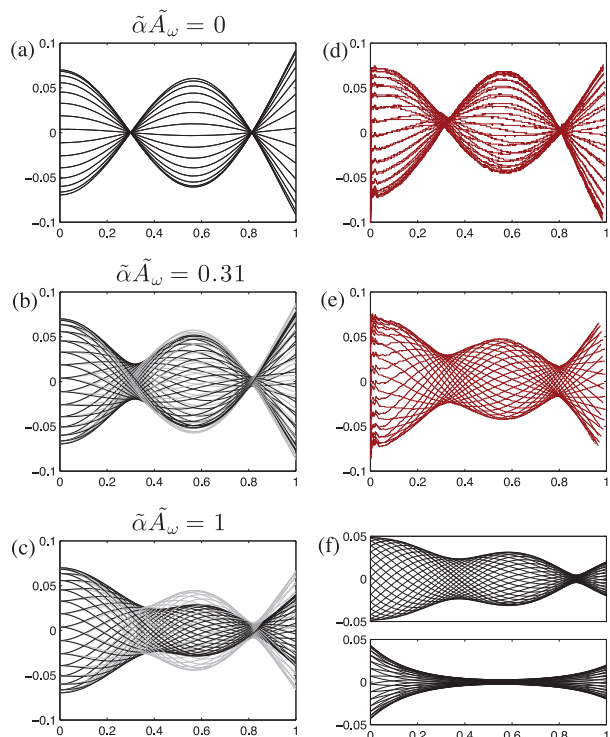


Fig. 2: (Colour on-line) Evolution of the plate response $y(x, t)$ as defined in eq. (7) for different rates of dissipation $\tilde{\alpha}\tilde{A}_\omega$ (the forcing is on the left side of the profiles). (a) and (d): $\tilde{\alpha}\tilde{A}_\omega = 0$ (no friction), the response is a standing-wave solution, classically observed for conservative systems. Left: solution of eq. (7) and right: experimental measurements (performed in air). (b) and (e): $\tilde{\alpha}\tilde{A}_\omega = 0.31$, the response is here no longer stationary due to the imbalance between forward and backward traveling waves. Again, left: solution of eq. (7) and right: experimental measurements (in water). The nonlinear solution of eq. (2) has been superimposed (light gray) for comparison and exhibits only slight differences. (c) and (f): $\tilde{\alpha}\tilde{A}_\omega = 1$ (strong friction). Nearly all the energy is now traveling in one preferred direction, resulting in an anguilliform kinematics. As can be seen from the nonlinear calculation, the friction is here overestimated. However, the physics observed remains similar. The right panel details the contributions of the first two terms of eq. (7) (top), and the other two (bottom).

[MovieS4.avi](#)). The nonlinear solution of eq. (2) has been superimposed for comparison (light gray), and it exhibits only slight differences with its linearized version. Finally, by further increasing the friction rate, a propagating wave kinematics is established (see fig. 2(c)). The comparison with the nonlinear direct calculation is here less accurate. As indicated before, the linearized version of the damping term overestimates the dissipation along the plate, explaining the observed deviation between both solutions and the more pronounced spatial amplitude attenuation. However, it is important to note that the global dynamics remains similar and that the observed differences do not interfere with the understanding of the mechanism for the transition.

Quantitatively, the continuous transition from a standing-wave solution to a traveling behavior can be observed by plotting the ratio of the energies related to the waves traveling forward and backward, as a function of the friction rate. This energy ratio $\bar{\mathcal{E}}$ is given by

$$\bar{\mathcal{E}} = \frac{\int_0^1 \int_0^{2\pi/\tilde{\omega}_f} [A_p^- e^{i(\tilde{\omega}_f t - k_r x)}]^2 dx dt}{\int_0^1 \int_0^{2\pi/\tilde{\omega}_f} [A_p^+ e^{i(\tilde{\omega}_f t + k_r x)}]^2 dx dt} = \frac{\int_0^1 [A_p^-(x)]^2 dx}{\int_0^1 [A_p^+(x)]^2 dx}. \quad (9)$$

Equation (9) is plotted in fig. 3(a) as a function of the damping rate $\tilde{\alpha}\tilde{A}_\omega$. The transition to the anguilliform traveling kinematics is here clearly exemplified. The system transits from a $\bar{\mathcal{E}} \sim 1$ regime (*i.e.* the amount of energy traveling forward and backward is equal) to $\bar{\mathcal{E}} \rightarrow 0$ (all the energy travels forward).

Figures 3(b) and (c) also show the evolution of the wave numbers k_r and k_i with $\tilde{\alpha}\tilde{A}_\omega$. k_r increases a little along the transition, meaning that the mode shape slightly changes due to the presence of strong damping slowing down the propagation (related to $v_{\phi,r}$, the real part of the phase speed). k_i (associated to the spatial attenuation length l_i) on the other hand, decreases from 0 to ~ -1.5 consistently with the increase of dissipation. Thus, we see that the presence of strong damping (*i.e.* $k_i \neq 0$) is a crucial ingredient in selecting the energy ratio that allows for propagation, thus determining how much the response will diverge from a standing-wave solution. From a physical point of view, a certain amount of energy is gradually extracted from the wave forward and further backward after the reflection as shown in fig. 3(d), that displays the energy per unit length $[A_p^\pm(x)]^2$ carried by each wave. $\tilde{\alpha}\tilde{A}_\omega$ modulates the decay rate, thus allowing to play on the imbalance of the amount of energies traveling in both directions. The nonlinear nature of the dissipation (proportional to ω_f^2) ensures a sufficiently fast dissipation rate (with respect to the other physical ingredients) to nearly mask the effect of the reflection. However, one has to note that in the present case, the fact that the removal of energy is continuous imposes a sort of coherence between both waves in the vicinity of the reflection point. As a consequence, the spatial envelope of the plate oscillations exhibits a narrowed zone at the tail, due to this interference (see figs. 2(b) and (c)). For actual real systems though, the presence of a fluid wake withdrawing a part of the incident wave energy might attenuate this effect (see fig. 2(e) that shows a less narrowed zone).

This work shows the mechanisms through which a traveling-wave global kinematics can be obtained even in very geometrically constrained media. The strong damping here modifies the system impedance by extracting energy all along the plate, which leads to an imbalance between incident and reflected waves. In the present context of aquatic propulsion, the establishment of an anguilliform kinematics has a direct consequence on the

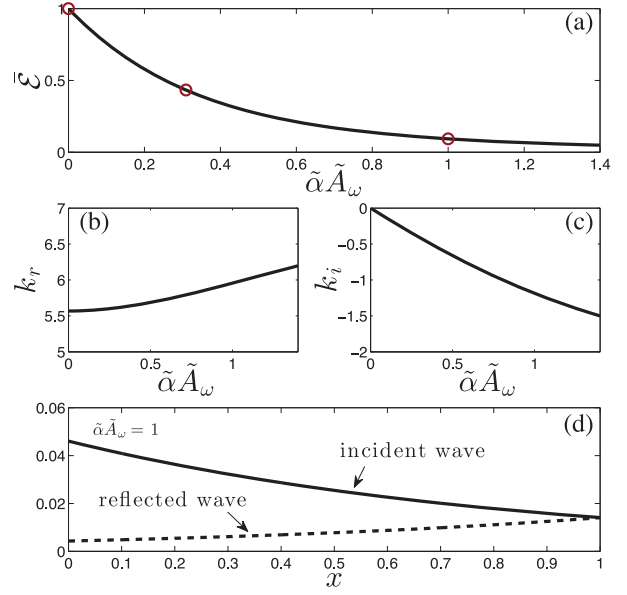


Fig. 3: (Colour on-line) (a) Evolution of the energy ratio $\bar{\mathcal{E}}$ as a function of the damping rate. The transition from standing-waves solutions ($\bar{\mathcal{E}} \sim 1$) to traveling kinematics ($\bar{\mathcal{E}} \rightarrow 0$) is here clearly exemplified. The three values of $\tilde{\alpha}\tilde{A}_\omega$ used in fig. 2 are indicated. (b) Evolution of the wave number k_r ; (c) the wave number k_i with $\tilde{\alpha}\tilde{A}_\omega$. (d) Wave energy ($[A_p^\pm]^2$) as a function of x for the incident (thick line) and reflected (thick dashed line) waves for the case $\tilde{\alpha}\tilde{A}_\omega = 1$ (to be compared with fig. 2(c)). As can be seen, the strong dissipation ensures a negligible contribution of the backward traveling wave to the global dynamics allowing the establishment of a propagative kinematics.

performance of artificial elastic swimmers (as described in [1]). As reported in the literature [2,3], the efficiency of the swimming movements η is directly related to the velocity of the wave traveling down the body v_ϕ : $\eta = \frac{1}{2}(1 + U/v_\phi)$ (where U is the swimming velocity). A progressive wave is thus desirable since it leads to efficiencies systematically higher than 1/2, and whose value is set by the speed ratio U/v_ϕ . Conversely, it has been shown that swimmers executing standing waves cannot exceed an efficiency of $\eta = 1/2$ [2]. The transition to anguilliform swimming by means of an appropriate source of dissipation is thus a way to optimize such systems. This mechanism also offers the advantage of being passive, which means that it does not require a complex active control of the undulatory motion. Regarding the particular point of optimization, the implementation of a spatially inhomogeneous damping is a promising option in order to increase the efficiency of the mechanisms described above. As discussed, homogeneous damping imposes a residual coherence between both traveling waves next to the reflecting end. A non-uniform damping could reduce the wave interference. For example, soft dissipation at the energy injection point and strong dissipation at the reflection point would increase the quality of the energy transfer. From a practical point of view, the inhomogeneous distribution of damping could

be implemented using a spatially varying thickness along the plate, the dissipation being proportional to the surface of the local cross-section. This might be helpful for the future design of artificial swimmers, for instance. It is worth noting that the results detailed in this study can be extended to any dynamical systems that can be described similarly to eq. (2). The possibility of adapting or drastically changing the kinematics is an interesting feature opening a large field of perspectives.

* * *

This work is supported by the EADS Foundation through project “Fluids and elasticity in biomimetic propulsion”.

REFERENCES

[1] RAMANANARIVO S., GODOY-DIANA R. and THIRIA B., *Proc. R. Soc. Interface*, **10** (2013) 20130667.

[2] LIGHTHILL J. M., *J. Fluid Mech.*, **9** (1960) 305.

[3] LIGHTHILL J. M., *J. Fluid Mech.*, **44** (1970) 265.

[4] WU T. Y., *J. Fluid. Mech.*, **46** (1971) 337.

[5] RAMANANARIVO S., GODOY-DIANA R. and THIRIA B., *Proc. Natl. Acad. Sci. U.S.A.*, **108** (2011) 5964.

[6] BARRETT D. S., *Propulsive Efficiency of a Flexible Hull Underwater Vehicle* (Massachusetts Institute of Technology) 1996.

[7] GABAI R. and BUCHER I., *J. Appl. Mech.*, **77** (2010) 021010.

[8] GABAI R. and BUCHER I., *J. Sound. Vib.*, **319** (2009) 406.

[9] MEIROVITCH L., *Analytical Methods in Vibration* (The Macmillan Company New York, NY) 1967.

[10] PAÏDOUSSIS M. P., *Fluid-Structure Interactions. Slender Structures and Axial Flow*, Vol. **2** (Academic Press, London) 2004.

[11] ELOY C., KOFMAN N. and SCHOUVEILER L., *J. Fluid Mech.*, **691** (2012) 583.

[12] BUCHAK P., ELOY C. and REIS P. M., *Phys. Rev. Lett.*, **105** (2010) 194301.